Response to Referee #1 Comments

This paper proposed a novel approach evaluating the soil erosion based on the rainfall dropsize distribution from WRF. Authors have addressed most of my comments. The only weak part is the discussion section. It would be completer and more meaningful if additional detailed comparisons with previous studies can be done to demonstrate the advantages of the proposed approach over the traditional approaches. Also it would be better to separate the discussion and conclusion section in my opinion. Other than this comment, the manuscript is good.

Response: The discussion and conclusion section were separated. The new conclusion section was rewritten as follows.

"This study presented a novel method for large-scale rainfall KE and erosivity estimation based on high-resolution, WRF-derived DSDs. Three microphysical parameterizations schemes (Morrison, WDM6, and Thompson aerosol-aware [TAA]) were designed to obtain raindrop size distributions, rainfall KE and rainfall erosivity for the entire of the UK covering the period of 2013–2017. With validation from the long-term observations of a disdrometer, the WRF-based rainfall erosivity exhibited an acceptable performance at Chilbolton station. Among the three WRF schemes, TAA exhibited the most superior performance and was recommended for future investigation. The results revealed that high rainfall erosivity occurred in the west coast area of the UK. Compared with the traditional empirical method, the proposed method can explain rainfall erosivity from a microphysical perspective and reflect more spatial variation because of changes in rainfall KE at the whole-country scale. Therefore, the development of a numerical weather prediction model offers an opportunity to better understand rainfall erosivity directly from its true definition. More importantly, because the WRF model is able to be driven by the global reanalysis data to obtain large-scale rainfall kinetic information, the proposed scheme can be easily applied to other regions, especially in ungauged areas.

Some problems remain with the proposed scheme, as discussed in section 5. Some of the problems, such as temporal downscaling of rainfall and point-to-area representative error by WRF, may introduce further uncertainty. This should be put in perspective of future work. It is expected that further exploration of research areas with different climatic and geographical characteristics would help us to establish a greater degree of accuracy on this matter."

In addition, the detailed comparisons with previous studies were added in the discussion section as follows:

"Compare to the previous large-scale rainfall erosivity studies based on empirical formula and spatial interpolation, this study presents a WRF-driven approach directly using the simulated rainfall microphysical variables. As demonstrated in the literatures, the relation between rainfall intensity and erosivity is not straightforward (Panagos et al., 2015a; Ballabio et al., 2017; Panagos et al., 2017). However, although all works show that rainfall erosivity decrease from west to east in UK, previous studies (Panagos et al., 2015a; Naipal et al., 2015) using traditional methods lead to an overestimation of rainfall erosivity, which may due to parameter *a* in the universal *KE–I* relationship is too high for the UK. Considering the five years (2013–2017) as a whole, the averaged $R_{W\text{-}Morrison}$, $R_{W\text{-}WDM6}$, and $R_{W\text{-}TAA}$-factor in each grid can be calculated. Nationally, the mean values of the three R_W-factors are 446.57, 640.92, and 416.35 MJ mm ha^{-1} h^{-1} y^{-1}, and their coefficients of variation (CV) are 0.56, 0.81, and 0.59, respectively. Compared with the outcomes (mean R-factor=746.6 MJ mm ha^{-1} h^{-1} y^{-1}, CV=0.81) of the Panagos et al. (2015a) using traditional methods, the R-factor of WDM6 scheme are quite similar, while other schemes have relatively low R-factors and low CVs."

Response to Referee #2 Comments

The discussion part of the paper can be further enriched. Better to separate the Discussion and Conclusion parts. The soil erosion yield is well known by its complexity and heterogeneity, especially at the field scale due to a large number of controlling factors and their interactions (such as surface roughness, land cover, soil properties etc.) during the erosive events. Benaud et al. 2020 (https://doi.org/10.1016/j.geoderma.2020.114378) is a very good example for that where the erosion rates between arable and grassland did not differ a lot considering different experiments conducted in different locations, times and for different purposes. However, under controlled conditions or theoretical framework (like the present study), the results look smoother, consistent and very promising. However, when they are confronted with the natural conditions (which are much complex), the conclusions change significantly. I still believe that the recent work of Benaud et al. 2020 (https://doi.org/10.1016/j.geoderma.2020.114378) can be used to validate the approach and/or (at least) enrich the discussion significantly. For instance, they clearly mentioned and showed how much the topsoil texture map (Fig. 3) could explain the spatial distribution and magnitude of soil erosion records of UK. Fig. 3 of Benaud et al. 2020 clearly also showed the correlation between the rainfall distribution (Rainfall distribution of UK) and soil erosion, which is very complementary to your statement. So, here I recommend the authors to emphasize the added value of this study to the soil erosion community by enriching the discussion part, significantly, considering the most relevant references.

Response: It is worth remarking that rainfall erosivity is not the soil eroding amount by rainfall, but a kind of erosion potential of the soil powered by rainfall kinetic energy. In terms of the influence of complex natural conditions such as vegetation, topography, and soil properties on soil erosion, they need to be considered in the soil erosion model. For example, the widely used RUSLE model takes into account these influences with six factors (rainfall erosivity factor R, soil erodibility factor K, soil length factor L, slope steepness factor S, cover management factor C, and supporting practices factor P). We suppose the comparison of soil erosion models is a significant research content but different from the aim of this work. In the future study, we will combine the WRF-derived rainfall erosivity results with the soil erosion model, and conduct an in-depth comparative analysis with Benaud et al. 2020 to investigate more physical mechanism of soil erosion.

The discussion and conclusion section were separated and additional detailed comparisons with

previous studies were added in the discussion section (see Response to Referee #1).

Estimation of rainfall erosivity based on WRF-derived raindrop size distributions

Qiang Dai[1, 2], Jingxuan Zhu[1], Shuliang Zhang[1], Shaonan Zhu[3], Dawei Han[2] and Guonian Lv[1]

[1]Key Laboratory of VGE of Ministry of Education, Nanjing Normal University, Nanjing, China.

[2]Department of Civil Engineering, University of Bristol, Bristol, UK.

[3]College of Geographical and Biological Information, Nanjing University of Posts and Telecommunications, Nanjing, China

Corresponding author: Qiang Dai (qd_gis@163.com)

Key Points:

- Rainfall kinetic energy derived from the Weather Research and Forecasting model offers a novel way to estimate large-scale soil erosion.
- Annual rainfall and erosivity are not always positively correlated.
- Highest rainfall erosivity of UK occurs in the west coast area during 2013–2017.

Abstract

Soil erosion can cause various ecological problems, such as land degradation, soil fertility loss, and river siltation. Rainfall is the primary water-driving force for soil erosion, and its potential effect on soil erosion is reflected by rainfall erosivity that relates to the raindrop kinetic energy. As it is difficult to observe large-scale dynamic characteristics of raindrops, all the current rainfall erosivity models use the function based on rainfall amount to represent the raindrops kinetic energy. With the development of global atmospheric re-analysis data, numerical weather prediction techniques become a promising way to estimate rainfall kinetic energy directly at regional and global scales with high spatial and temporal resolutions. This study proposed a novel method for large-scale and long-term rainfall erosivity investigations based on the Weather Research and Forecasting (WRF) model, avoiding errors caused by inappropriate rainfall–energy relationships and large-scale interpolation. We adopted three microphysical parameterizations schemes (Morrison, WDM6, and Thompson aerosol-aware) to obtain raindrop size distributions, rainfall kinetic energy and rainfall erosivity, with validation by two disdrometers and 304 rain gauges around the United Kingdom. Among the three WRF schemes, Thompson aerosol-aware had the best performance compared with the disdrometers at a monthly scale. The results revealed that high rainfall erosivity occurred in the west coast area at the whole country scale during 2013–2017. The proposed methodology makes a significant contribution to improving large-scale soil erosion estimation and for better understanding microphysical rainfall–soil interactions to support the rational formulation of soil and water conservation planning.

1 Introduction

Soil erosion plays a pivotal role in shaping the Earth's physical landscape; however, it can threaten both ecosystems and human societies (Alewell et al., 2015). Accurate quantification of soil loss impact at large spatial scales is therefore important for developing land-use planning and sustainable conservation practices (Bilotta et al., 2012). The soil erosion rate is driven by a combination of factors, including rainfall, topography, soil characteristics, land cover, and land management applications (Wischmeier and Smith, 1958; Panagos et al., 2015b). Among these, rainfall is a driving force that accounts for a large proportion of soil loss throughout most of the world (Panagos et al., 2015b). The erosive force of rainfall with consequent runoff is represented

as erosivity of rainfall. This is a crucial factor for estimating soil loss in large-scale soil erosion models; for instance, the Universal Soil Loss Equation (USLE (Wischmeier and Smith, 1978) or RUSLE (Renard et al., 1997)), Limburg Soil Erosion Model (LISEM) (De Roo et al., 1996), and USLE-M (Kinnell and Risse, 1998).

Rainfall erosivity estimation involves the microphysical properties of rainfall and rainfall–soil interactions on different time steps (Petan et al., 2010). Impact of rainfall, the main mechanism driving the splashing of soil particles from the soil mass, which leads to soil erosion through soil disintegration and mobilization, relies on the kinetic energy (KE) of raindrop motions (Wischmeier and Smith, 1958; Wang et al., 2014). Robust measurement of raindrop size and terminal velocity is vital for estimating and predicting rainfall erosivity. Many measurements can be used to obtain these two parameters, including the stained paper or flour pellet methods (Marshall and Palmer 1948; Wischmeier and Smith, 1958), high speed cameras (Jones, 1959; Kinnell, 1981; McIsaac, 1990), and disdrometers (Petan et al., 2010; Angulo-Martinez et al., 2012). Accurate measurements of raindrop size can be provided in all their methods, and terminal velocity of raindrops can be further measured by video cameras and disdrometers. Velocity can also be estimated as the function of raindrop diameter from the empirical relationship (Beard, 1976; Atlas and Ulbrich, 1977; Uplinger, 1981; Van Dijk et al., 2002). When using ground observations, rainfall KE can be estimated at a given site.

However, direct measurement of rainfall KE in a large area is difficult because it requires considerable effort, as well as a dense network of expensive instruments that provide accurate outputs (Fornis et al., 2005; Mikoš et al., 2006; Meshesha et al., 2016; Dai et al., 2017). Previous studies have, therefore, mainly employed more readily accessible records like rainfall intensity, and attempted to estimate rainfall KE from the empirical relationship of unit KE (*ke*) with intensity (*ke–I*). Since Marshall and Palmer (1948) first observed a two-parameter exponential relationship between drop size and intensity, several forms of *ke–I* mathematical expressions for specific locations and climatic conditions have been proposed, including power-law (Park et al., 1982; Meshesha et al., 2016), linear (Sempere-Torres et al., 1998; Nyssen et al., 2005), polynomial (Carter et al., 1974), logarithmic (Wischmeier and Smith, 1978; Davison et al., 2005; Meshesha et al., 2014), and exponential (Kinnell, 1981; Brown and Foster, 1987) relationships. Among these, the exponential function has been preferentially used currently (Van Dijk et al., 2002; Fornis et al., 2005; Petan et al., 2010; Sanchez-Moreno et al., 2012; Lim et al., 2015). Accurate raindrop size

distribution (DSD) measured by disdrometers is widely used to derive *ke–I* relationships (Angulo-Mart ńez et al., 2016; Meshesha et al., 2016). However, such empirically derived formulas indicate that rainfall *ke* will increase infinitely with increasing intensity, whereas studies (Rosewell, 1986; Angulo-Mart ńez et al., 2016; Meshesha et al., 2019) have found that rainfall *ke* reaches an top value when intensity is around 70 mm h^{-1} (Hudson, 1963; Wischmeier and Smith, 1978). More importantly, such a *ke–I* relationship only represents local climate and precipitation microphysics and is valid for such regions. There is great uncertainty associated with rainfall erosivity estimation using this *ke–I* relationship in a large domain (Angulo-Mart ńez and Barros, 2015), especially due to the poor spatial and temporal predictability of the *ke–I* relationship. This has motivated researchers to directly calculate KE based on large-scale DSD measurements.

Ground- and space-based radar can be used to obtain DSD parameters (Atlas et al., 1973; Doelling et al., 1998). For example, the space-borne Dual-frequency Precipitation Radar (DPR) radar containing Ku- and Ka-bands in the Global Precipitation Measurement (GPM) satellite allows researchers to estimate the global three-dimensional spatial distribution of hydrometeors. Unfortunately, ground dual-polarization radars are available in limited areas (Prigent, 2010) with large uncertainties (Dai et al., 2019), and the GPM DPR instrument, which measures DSD with daily or longer temporal resolutions, fail to capture a full storm and meet the requirement for rainfall kinetic estimation. Mesoscale numerical weather prediction models, for instance, the WRF model, can simulate microphysical cloud processes and predict the evolution of particle size distribution through computationally feasible parametrization schemes (Dai et al., 2014; Brown et al., 2016). DSD on the ground can be derived from the WRF model through consideration of various physical processes, types of hydrometeor, and free degrees of size distributions in hydrometeor. As such, a number of recent researches have investigated the retrieval and uncertainty of DSD parameters by WRF (Gilmore et al., 2004; Ćurić et al., 2009; Brown et al., 2016; Yang et al., 2019).

The WRF model runs with initial and boundary conditions using global reanalysis datasets, such as those of the European Centre for Medium-range Weather Forecasts (ECMWF) and National Centers for Environmental Prediction (NCEP). In other words, WRF-derived DSD can be obtained for any given area with fine spatial and temporal resolutions rather than traditional course linear interpolations. We therefore attempted to estimate rainfall erosivity for the entirety of the United Kingdom (UK) domain using WRF-derived DSD. For comparison, we also

calculated interpolated traditional disdrometer-derived rainfall erosivity. To our knowledge, this work is the first attempt to take advantage of a numerical weather prediction model for estimating rainfall erosivity anywhere around the world. The current study contributes to the development of large-scale soil erosion estimation and provides a better comprehension of microphysical rainfall–soil interactions.

2 Methodology

2.1 Disdrometer-based rainfall KE estimation

KE dominates the ability of raindrops to separate soil particles. The KE (e, unit: J) of a raindrop with mass m (g) and terminal velocity v (m s^{-1}) is defined by:

$$e = \frac{1}{2} m v^2 \tag{1}$$

Assuming a spherical volume for every raindrop shape, the mass of a drop can be calculated from the cube of the diameter D (mm). Because instruments (e.g., disdrometers) generally sample drop size, the mean radius and falling velocity of the corresponding sampling drop-size class are used to represent D and v, expressed as D_i and v_i, respectively. In such cases, the e_i with any drop of a given class is given as:

$$e_i = \frac{1}{12} 10^{-6} \pi \rho v_i^{\,2} D_i^{\,3} \tag{2}$$

where ρ is the water density (g cm^{-3}). The sum of the KE of each individual raindrop within a given rain depth that hits a given area defines the total KE. The unit rainfall KE ke_t in the t^{th} minute (MJ ha^{-1} mm^{-1}) can be calculated as the sum of each drop KE in each size set, as follows:

$$ke_t = \frac{e_{sum}}{AP_t} = \frac{1}{AP_t} \sum_{i=1}^{ni} N_i e_i \tag{3}$$

where A represents the sample area of the sensor, P_t is rainfall depth at time t, and N_i is the drops number in class i. The instrument sums up the number of raindrops in each sampling class and produces the raindrop spectra for a time step. Here, we use the term *ke* to represent the disdrometer-based KE estimated by DSD directly measured every minute. The terminal velocity of a raindrop

can be estimated from its power law empirical relationship with raindrop diameter (Atlas and Ulbrich, 1977), with this considered more suitable for Chilbolton in the UK (Islam et al., 2012):

$$v_{Atl} = 3.78 D_i^{0.67} \quad (4)$$

Thus, unit rainfall KE estimates per minute are obtained by replacing v_i in Eq. (2) with v_{Atl}.

The other form of rainfall KE is expressed at an event scale and represents the sum of the storm energy covering all time steps covering an event. The individual event energy (MJ ha^{-1}) is calculated as follows:

$$E = \sum_{t=1}^{nt} k e_t P_t \quad (5)$$

where P_t is the rainfall amount (mm) in the t^{th} minute and nt is the time steps number. Historical rainfall data are divided into wet and dry periods. A string of erosive rainfall storms is first extracted through the predefined rules. A continuous 6-h dry period interval was used to divide rainfall events (Hanel et al., 2016), following the "minimum dry-period duration" definition of a rainfall event (Bonta, 2004). Moreover, a rainfall amount of 12.7 mm was set as the threshold to filter effective rainfall events (Renard et al., 1997).

Rainfall KE is obtained for a given site based on size and velocity of raindrops. When disdrometer data are absent, energy can be estimated from empirical relationships using rainfall intensity I (mm). Five commonly used functions (including exponential, logarithmic, power law, and inverse proportion) have been mentioned in Section 1. Taking the exponential form as an example, the rainfall KE at any location can be estimated as:

$$E_{\max} = e_{\max}(1 - ae^{-bI}) \quad (6)$$

where e_{max} is the mean maximal value of energy measured under high rainfall intensity, and a and b are coefficients modeling the equation curve. Here, minimum KE can be determined by parameters a and e_{max} together, while the overall shape of the curve is modeled by parameter b.

2.2 WRF-based rainfall KE estimation

Differing from disdrometer measurements, the complete DSD cannot be obtained from the WRF model. Instead, the DSD of the microphysical parameterization (MP) scheme is handled with a constrained-gamma distribution model, which is defined as:

$$N(D) = N_0 D^{\mu} e^{-\lambda D} \tag{7}$$

where N_0, μ, and λ are the intercept, shape, and slope parameters of the DSD. In terms of double-moment bulk schemes, N_0 and λ can be abstracted from the number concentration N and predicted mixing ratio q, as shown below:

$$N_0 = \frac{N\lambda^{\mu+1}}{\Gamma(\mu + 1)} \tag{8}$$

$$\lambda = \left[\frac{cN\Gamma(\mu + d + 1)}{q\Gamma(\mu + 1)}\right]^{\frac{1}{d}} \tag{9}$$

c and d are the assumed power-law coefficients between diameter and mass ($m = cD^d$), and Γ represents the function in gamma form (Morrison et al., 2009). The value of the shape parameter μ ($\mu = 0$) in double-moment schemes is fixed, except for the WRF double-moment 6-class (WDM6) schemes, following gamma distribution, which defined $\mu = 1$ (Jung et al., 2010; Johnson et al., 2016).

Because DSD retrieval is sensitive to MPs (Cintineo et al., 2014; Morrison et al., 2015), the WRF model this study adopted completely or partially three types of double-moment cloud MP schemes. The Morrison double-moment scheme involves the number concentrations and mixing ratios of multiple hydrometeors (Morrison et al., 2009). Moreover, the WDM6 scheme further considers a prognostic factor to estimate and predict the cloud condensation nuclei (CCN) number concentration (Hong et al., 2010; Lim and Hong, 2010). Finally, the Thompson aerosol-aware (TAA) scheme can predict both ice nuclei (IN) and CCN number concentrations (Thompson and Eidhammer, 2014).

The DSD parameters were thus obtained under the three WRF MPs. For theoretical DSD, *ke* estimates per minute were obtained by integration of the full raindrop size spectrum using:

$$ke'_t = \frac{1}{AR_t}\int_0^{\infty} N(D)\frac{1}{12}10^{-6}\pi\rho v_i^{\,2}D_i^{\,3}dD \quad (10)$$

For the WRF-derived DSD covering the whole study area, there was no need to construct a *ke*–I relationship to interpolate KE in ungauged areas. The WRF-based rainfall KE under storm event scale is thus given as:

$$E_W = \sum_{t=1}^{nt} ke'_t\ P_t \quad (11)$$

2.3 Rainfall erosivity estimation

Most storm events have relatively low intensities and KEs with occasional peaks, based on the disdrometer DSD data used to evaluate the rainfall *ke–I* function. Proper estimation of rainfall erosivity potential should consider total KE over a long period. The rainfall erosivity factor (or R-factor) is calculated by a multi-annual average of the total storm erosivity index (Wischmeier and Smith, 1958; Van Dijk et al., 2002), while annual rainfall erosivity *R* can be obtained using:

$$R = \sum_{m=1}^{M}(EI_{30})_m \quad (12)$$

where *M* is the total number of erosive events within a year. $(EI_{30})_m$ are total rainfall kinetic energy and maximum 30-min rainfall intensity recorded within 30 consecutive minutes (unit: mm h^{-1}), respectively, for the m^{th} event.

Wischmeier and Smith (1958) first proposed the use of EI_{30}, as the rainfall erosivity for each event, based on research data from many sources. I_{30} was calculated to have higher relevance to soil erosion than maximum 5-min, 15-min, or 60-min rainfall intensities (Wischmeier and Smith, 1958). The calculation of EI_{30} initially uses recording-rain gauge data to divide continuous rainfall into time periods with equal rainfall intensity. Though rainfall measurements with high temporal resolutions are required, it is difficult to obtain them from general rainfall measurements. Therefore, short time equal-interval rainfall data with higher accuracy over multiple years are preferred for estimating EI_{30}. For example, Xie et al. (2016) used 1-min rainfall data instead of recording-rain gauge records. For coarse-resolution, equally spaced data, researchers have proposed a conversion factor to reduce bias error (Weiss, 1964; Williams and Sheridan, 1991).

The rainfall erosivity can be derived from rainfall KE. It plays a main dynamic role in USLE/RUSLE, representing the potential for soil erosion caused by rainfall. To distinguish the disdrometer- and WRF-derived rainfall erosivity in this study, we use the terms R_D and R_W, respectively.

2.4 Evaluation methods

Because there is no direct way to measure rainfall erosivity across a large area, it is difficult to validate outcomes using observations. However, R_D is considered to be relatively accurate due to its specific measurement of raindrops. We therefore assumed that R_W values were accurate if it closely matched R_D of a given location. A long-term comparison of R_W and R_D at disdrometer stations was thus conducted to evaluate the validity of R_W.

Three indicators were introduced for the evaluation: Pearson's correlation coefficient, mean absolute error (MAE), and coefficient of determination (R^2) (Borrelli et al., 2017). Pearson correlation coefficient is an index used to evaluate the linear correlation between two variables, and is defined as follows:

$$Pearson = \frac{n\sum R_{D_i}\sum R_{W_i} - \sum R_{D_i}\sum R_{W_i}}{\sqrt{n\sum {R_{D_i}}^2 - (\sum R_{D_i})^2}\sqrt{n\sum {R_{W_i}}^2 - (\sum R_{W_i})^2}} \quad (13)$$

where n is the number of variable samples. Because this correlation cannot reveal the absolute bias of rainfall erosivity values, the MAE was also used; this is defined as:

$$MAE = \frac{\sum \left| R_{W_i} - R_{D_i} \right|}{n} \quad (14)$$

R^2 is an indicator to assess the fit of the trend line, expressed as the ratio of the variance in the dependent variable predicted from the independent variable. It measures the extent to which the model replicates observations based on the proportion of the results interpreted by the model to the total change, written as:

$$R^2 = 1 - \frac{SS_{res}}{SS_{tot}} \quad (15)$$

where SS_{res} is the sum of squares of residuals between two variables, and SS_{tot} is the total sum of squares.

3 Study area and data sources

The whole of the UK was set as the experimental area for investigating rainfall erosivity estimation. The UK consists of mostly lowland terrain, with a maximum elevation of 1345 m. Water and wind are the most significant forces of soil erosion in the UK. Together, they cause approximately 2.2 million tons of topsoil to be eroded annually, seriously affecting soil productivity, water quality, and aquatic ecosystems through siltation of watercourses (EA, 2004). According to the Environmental Agency, the total cost of soil erosion in the UK is approximately $88 million each year, including an agricultural production loss of $17.6 million (O'Neill, 2007). More importantly, the changing climate may exacerbate the degree of erosion. For example, hotter, drier climates make soils more susceptible to wind erosion, and intense storms increase rainfall erosivity (Defra, 2009). Studies of water erosion in England and Wales (Morgan, 1985; Evans, 1990) have found that loose soils (especially sand), such as the soils found in Shropshire and Herefordshire in Wales, are more susceptible to water erosion. In a study of rainfall erosion in Europe, Panagos et al. (2015a) found that the humid Atlantic climate results in highly variable rainfall erosivity, such as higher R-factor values in western England and lower values in the eastern UK.

The gauge datasets used are from the land surface and marine surface measurements datasets (data availability: 1853–present) provide by the UK Met Office. A network of rain gauges covering 304 stations across the whole UK observes continuous rainfall data in hours (Figure 1). The base data of most stations comprises the times of each tip (0.2 mm per tip), converted into 1-h rain accumulations. The rainfall observations are not always valid for each hour at each station. The hourly grid-based rainfall maps are then calculated based on ordinary kriging interpolation of rain gauge network data to obtain the spatial distribution of rainfall for each time step, as inputs for rainfall erosivity estimation. This wide-range-use geostatistical approach can account for both the distance and pairwise spatial relationship between points through variograms. The precipitation interpolation method uses sample gauge points taken at different locations and creates a continuous surface to achieve an accurate spatial variation estimation of rainfall patterns.

We used data from two disdrometers in southern England. The first was Chilbolton station (51°08'N, 1°26'W), with an impact-type Joss–Waldvogel disdrometer (JWD) mainly used to compute rainfall erosivity. It can measure drop sizes from 0.3 to 5.0 mm in 127 bins. The sampling

period and collector area were 10 s and 50 cm^2, respectively. Data were available for April 2003 to July 2018. The second was the University of Bristol station (51 °27'N, 2 °36'W), with an OTT Parsivel^2 disdrometer (OPD). Data were available for November 2015 to December 2018. This disdrometer subdivides particles into appropriate classes and has a nominal cross-sectional area of 54 cm^2. The 10-s period measurement data from the two disdrometers were averaged into a 1-min period to filter out time variations (Montopoli et al., 2008; Islam et al., 2012; Song et al., 2017).

Meteorological data comes from the ERA-Interim dataset, a global atmosphere re-analysis product, generated by the ECMWF. For the scientific community, ERA-Interim is considered to be one of the most important atmospheric datasets, with its data-rich period available since 1979 and updated in current time (Dee et al., 2011). The Integrated Forecasting System released in 2006 contains a 12-h analysis window derived 4-D variational analysis, driving the data assimilation system to generate ERA-Interim. The dataset covers 60 vertical classes of approximately 80 km from the ground to 0.1 hPa. The Gridded Binary format is used to store data for three months in a separate file. A data processing scheme was established to collect and retrieve ERA-Interim data of each rainfall event.

The rain gauge and Chilbolton disdrometer datasets can be obtained from British Atmospheric Data Centre in National Centre for Atmospheric Science research center (MO, 2012). ERA-Interim data can be obtained from the ECMWF Public Dataset website (https://apps.ecmwf.int/). Considering the availability of the above datasets and model requirements, we mainly used data covering the period 2004–2017.

4 Results

4.1 Empirically derived rainfall erosivity estimation

To evaluate the R_W, the raindrop spectrum collected by the Chilbolton station disdrometer is used to estimate rainfall KE first. The key in estimating rainfall KE by disdrometer lies in building an empirical relationship between rainfall amount and KE. We used DSD measurements from 2004 to 2013 to establish five empirical relationships between unit rainfall kinetic energy (*ke*) and intensity (*I*) (Table 1) and used 2014–2017 data for the cross-validation. It can be seen from Table 1 that the inverse proportional relationship (Equation III) had the worst performance, in that both the calibration and validation R^2 values were < 0.3. The values of the other equations were >

0.48, among which the exponential formula (Equation I) had the highest calibration R^2 (0.50) and validation R^2 (0.45), respectively. In addition, the power law formula (Equation V) showed a similar performance to the exponential formula at rainfall intensities < 5 mm h^{-1}. However, the power law formula also had a continuously increasing trend, which may not be suitable for high-intensities. Figure 2 shows the *ke–I* relationship and five fitted curves at Chilbolton station. It can be seen that the two logarithmic curves (Equation II and IV) invariably overlap. The logarithmic form has been used for a long time in USLE (Wischemier and Smith, 1978). It describes *ke* well at both low and high *I*, but does not have an upper limit. The power law curve (Equation V) can predict *ke* well at lower *I* but overestimates *ke* at high *I*. The exponent-based relationship (Equation I) is widely used in the literature and in forecast models such as RUSLE (Renard et al., 1997), which fits the data particularly well in Figure 2. Even though *ke* in exponential curve has a minimum value at very low *I*, it also should be noted that higher rainfall intensities are much more important in determining overall storm energy than lower intensities. Therefore, we adopted it here as the empirical formula to estimate rainfall erosivity in the UK.

Based on rainfall KE, the point R_D can be obtained at a disdrometer location. In the current study, we established a method to estimate the *R* using 60-min rainfall data. EI_{30} obtained from 1-min DSD data was considered as the standard *R* at Chilbolton Station. Hourly rain gauge data at the same location were used to calculate $(EI_{30})_{60}$, which refers to EI_{30} calculated from 60-min data. The regression relationship between EI_{30} and $(EI_{30})_{60}$ was then established. The $(EI_{30})_{60}$ of each month, obtained from the 60-min rainfall data of the Chilbolton Station rain gauge in 2004–2013, was calculated. The regression relationship between the monthly sum of $(EI_{30})_{60}$ and the standard monthly EI_{30} from DSD was calculated to obtain a coefficient of 1.836. Rainfall erosivity can subsequently be calculated by multiplying $(EI_{30})_{60}$ by the coefficient.

Beyond assuming that the disdrometer-derived *ke–I* relationship can be applied to a whole study area; point rainfall measurements must be interpolated to obtain areal rainfall values in traditional rainfall erosivity estimation. We obtained 60-min rainfall data from 304 rain gauges around the UK from 2004 to 2017. Note that not all rain gauges were available for the whole period (available gauges each year are indicated in Figure 3). We used the ordinary kriging interpolation method to obtain the spatial distribution of rainfall for each time step. This wide-range-use geostatistical approach can account for both the distance and pairwise spatial relationship between points through variograms. Figure 3 shows the results of annual rainfall (*Rain*), annual rainfall

kinetic energy (E), and annual rainfall erosivity (R) for different years. The distribution trends of *Rain*, E, and R were similar, and positively correlated except for certain locations or periods. For instance, in 2013, *Rain* in the northwestern UK decreased from west to east, while E and R decreased from south to north; furthermore, areas with large E and R values in southeastern UK could not be directly observed from the rain map.

The key concern in traditional rainfall erosivity estimation is the spatial predictability of the *ke–I* relationship. To verify the regional reliability of this relationship, we used data from a newer disdrometer located at the University of Bristol, approximately 87 km from Chilbolton Station. The validation data at Bristol Station discontinuously covered the period 2016–2019. Figure 4 shows the exponential relationship of *ke–I* at Bristol station, which differed substantially from that based on data from Chilbolton station. A comparison of the modeled and observed event rainfall erosivity is shown in Figure 5. The modeled erosivity of rainfall event was not consistent with the observed event rainfall erosivity. The linear regression coefficient between these values was > 1.2, which was the result of the low *ke* for Bristol Station, and R^2 was < 0.85, indicating considerable uncertainty associated with disdrometer-based rainfall erosivity estimation.

In summary, the point rainfall erosivity estimated by disdrometer is considered to be accurate compared to other methods. However, a large-scale rainfall erosivity through a simple interpolation of rainfall KE is subjected to a significant uncertainty. In the following analysis, the point R_D is used to appraise the performance of the proposed WRF-based estimated method, and the R_D in the whole UK is only be used for a general comparison of spatial and temporal distribution of rainfall erosivity.

4.2 Rainfall and DSD estimation by WRF

We used the WRF model ver. 3.8, which has an Advanced Research WRF dynamical core, to downscale the ERA-Interim reanalysis data. The double-nested domain configuration used in the WRF model was centered at 55 °19'N, 2 °21'W and applied at a downscaling ratio of 1:5, a finest grid of 5 km, and a temporal resolution of 1 h. Table 2 lists the detailed parameters used in this domain configuration. With the top pressure level set at 50 hPa in each, both domains include 28 vertical levels. To obtain favorable initial weather conditions, the model ran continuously to obtain five years of WRF simulation results.

Simulations were performed using three different bulk double moment MPs: the Morrison (Morrison et al., 2009), WDM6 (Hong et al., 2010; Lim and Hong, 2010) and TAA (Thompson and Eidhammer, 2014) schemes. All three can predict the number concentration and hydrometeors mixing ratio for each time step. The WDM6 scheme also predicts the number concentration of CCN (Hong et al., 2010; Lim and Hong, 2010), while the TAA scheme are able to predict both IN and CCN number concentrations (Thompson and Eidhammer, 2014). Additionally, other physical parameterizations include the Dudhia shortwave radiation scheme (Dudhia, 1989), Mellor–Yamada–Janjic planetary boundary layer scheme (Janjić, 1994), RRTM longwave radiation scheme (Mlawer et al., 1997), the Noah land-surface model (Ek et al., 2003), and the Kain–Fritsch cumulus scheme (Kain, 2004),.

The median volume diameter parameter (D_0) and generalized intercept parameter (N_w) are generally used in the DSD model of WRF (Islam et al., 2012).

$$N_w = \frac{N_0 D_m^{\mu}}{f(\mu)} \tag{16}$$

$$f(\mu) = \frac{6(4 + \mu)^{\mu+4}}{4^4 \Gamma(\mu + 4)} \tag{17}$$

where D_m is the mass-weighted mean diameter. The $f(\mu)$ is a function of the shape parameter μ. The parameter μ is assumed as zero or one (based on microphysical scheme configuration) in WRF. Figure 6 displays the spatial distribution of D_0 and generalized intercept parameter N_w for a given day with rainfall countrywide (January 10, 2013). D_0 and N_w had similar patterns and were mainly distributed across the southwestern and northeastern UK. The white strip in the middle of Figure 6 represents an area that received no rain. However, the three MPs yielded large differences; D_0 of MP-TAA was the highest among three MPs, whereas N_w of MP-WDM6 was significant larger than the others. In addition, D_0 and N_w did not consistently show a positive correlation. The different MP estimation results underscore the complexity of the rainfall process, which is the reason we estimated rainfall KE using WRF schemes instead of traditional formulas.

4.3 Comparison of WRF- and disdrometer-derived rainfall erosivity at Chilbolton station

With the WRF-based rainfall intensity and DSD estimations, rainfall erosivity was derived using Equations (10)–(12). Hereafter, this is referred to as R_W, which is further distinguished based

on the three MP schemes used: $R_{W\text{-}Morrison}$, $R_{W\text{-}WDM6}$, and $R_{W\text{-}TAA}$. Figure 7 compares disdrometer- and WRF-derived monthly rainfall erosivity estimations at Chilbolton station for the period 2014–2017. The general patterns of the four rainfall erosivity values were similar. $R_{W\text{-}Morrison}$ tended to be larger than R_D in some months, whereas $R_{W\text{-}TAA}$ matched the R_D value relatively well for smaller values. Because WRF data were taken from a 2 ×2-km grid around Chilbolton station, there was a spatial error in addition to the systematic error of estimating rainfall erosivity. Based on the four-year data, the study area is rainy throughout the year with little R monthly, or seasonal patterns change (Figure 8), influenced by the temperate oceanic climate. Figure 8 also indicated that through the perspective of monthly average results, $R_{W\text{-}WDM6}$ values are low, $R_{W\text{-}TAA}$ has a good similarity with low R_D, and $R_{W\text{-}Morrison}$ is the closest to R_D in value.

Table 3 shows the correlation indicator results between monthly R_D and the three types of R_W at Chilbolton station. The Pearson correlation coefficients generally exceeded 0.7, supporting the potential utility of WRF-based estimation. In terms of MAE, $R_{W\text{-}TAA}$ had the best performance (6.51), whereas $R_{W\text{-}Morrison}$ and $R_{W\text{-}WDM6}$ showed slightly worse performance (approximately 8). Among the three schemes, $R_{W\text{-}TAA}$ had the best fit with R_D. The indicators and comparison results suggest that the deviations in results need to be considered; therefore, a method of bias elimination is described in Section 4.4.

4.4 R_W estimation for the whole UK

The R_W at Chilbolton station showed obvious systematic deviations compared with the disdrometer-derived results (see Section 4.2 and 4.3). Simple bias correction was therefore applied to adjust the individual storm KE estimations of R_W. The biases from dividing average $R_{W\text{-}Morrison}$, $R_{W\text{-}WDM6}$, and $R_{W\text{-}TAA}$ by average R_D during 2014-2017 were 0.55, 0.20, and 0.36, respectively.

The rainfall erosivity distribution for the whole UK was then obtained. Figure 9 shows the distribution of R_W at the annual scale covering the period 2013–2017. The pattern of the rainfall erosivity maps showed a general regional-dominant characteristic. For example, it always decreased from west to east, predominantly shaped by orography. Affected by the prevailing westerly winds, there was abundant rainfall in the western and northern mountains, as indicated by high rainfall KE values in these regions. In addition, among the study years, 2014 and 2015 showed higher national rainfall erosivity, with a large range in the west coast area.

Figure 10 shows the average R distribution for 2013–2017 estimated by rain gauges and WRF MPs. WRF grids could cover all regions in the UK evenly, offering more detailed erosivity results, especially in the mountainous northwestern region. Here, values of average R map calculated by rain gauges were much higher than three types of R_W, although they all have R decreased from west to east. Noted that *ke–I* empirical equation at Chilbolton station used in the whole UK, will not always be accurate in regions with different rainfall characteristics. In terms of R_W results, the three MPs obtained the same spatial pattern in rainfall erosivity, where $R_{W\text{-}WDM6}$ yielded the greatest geographical difference. It is clear that the proposed WRF-based estimated method can capture more details of the spatial change of rainfall erosivity compared with the traditional disdrometer-based method.

The highest rainfall erosivity regions in the UK are concentrated in the mountainous areas along the western coast, related to their rainfall system. The moist air brought by the prevailing westerly wind from the Atlantic Ocean moves from west to east across the UK and rises when it encounters the mountains of western England. Therefore, the mountainous regions along the UK western coast have the highest rainfall amount and rainfall erosivity in the UK. In addition, western Scotland is under the subpolar oceanic climate, which enhances its humidity. On the contrary, eastern Scotland and northeastern England are more likely to expose continental polar air mass, which brings dry and cold air and lower rainfall erosivity.

To evaluate the change in rainfall erosivity with time in the UK, the average value of all the WRF grids covering the whole UK was calculated over 2013–2017 (Figure 11). The average R_W trends of $R_{W\text{-}Morrison}$ and $R_{W\text{-}TAA}$ were similar, both increasing from a minimum in 2013 to a maximum in 2014, and then gradually decreasing from 2014 to 2017. The red line in Figure 11 indicates a series of mean values of the three MPs results, which varied from 367.82 to 516.00 MJ mm ha^{-1} h^{-1} y^{-1} (mean: 432.16 MJ mm ha^{-1} h^{-1} y^{-1}).

The maximum values for $R_{W\text{-}Morrison}$ and $R_{W\text{-}TAA}$ occurred in 2014, whereas that of $R_{W\text{-}WDM6}$ occurred in 2015. A sequence of extreme weather events occurred in the UK in 2014, including major winter storms in late January to mid-February, which caused widespread flooding and other economic losses, and greatly increased rainfall erosivity that year. However, the gauge-based interpolation map shows the average annual rainfall amount for the years 2013–2017 were 884.9, 1014.0, 1008.5, 894.9, and 937.3 mm, respectively. The large rainfall erosivity difference between

2014 and 2015, and the two years with similar rainfall amount, indicates that much rainfall erosion occurs during the rainfall events of high intensity instead of simply high rainfall amount. A more notable variation pattern of rainfall erosivity may be found with longer simulation. The strength of the proposed method lies on its ability to estimate large covering and long-term rainfall erosivity.

5 Discussion ~~and conclusions~~

Compare to the previous large-scale rainfall erosivity studies based on empirical formula and spatial interpolation, this study presents a WRF-driven approach directly using the simulated rainfall microphysical variables. As demonstrated in the literatures, the relation between rainfall intensity and erosivity is not straightforward (Panagos et al., 2015a; Ballabio et al., 2017; Panagos et al., 2017). However, although all works show that rainfall erosivity decrease from west to east in UK, previous studies (Panagos et al., 2015a; Naipal et al., 2015) using traditional methods lead to an overestimation of rainfall erosivity, which may due to parameter a in the universal $KE–I$ relationship is too high for the UK. Considering the five years (2013–2017) as a whole, the averaged $R_{W\text{-}Morrison}$, $R_{W\text{-}WDM6}$, and $R_{W\text{-}TAA}$-factor in each grid can be calculated. Nationally, the mean values of the three R_W-factors are 446.57, 640.92, and 416.35 MJ mm ha^{-1} h^{-1} y^{-1}, and their coefficients of variation (CV) are 0.56, 0.81, and 0.59, respectively. Compared with the outcomes (mean R-factor=746.6 MJ mm ha^{-1} h^{-1} y^{-1}, CV=0.81) of the Panagos et al. (2015a), the R-factor of WDM6 scheme are quite similar, while other schemes have relatively low R-factors and low CVs.

Although an acceptable rainfall erosivity estimation is obtained using the WRF model, some uncertainties associated with it cannot be ignored. For example, as the MPs of WRF were closely related to DSD, improper determination of MPs will introduce additional uncertainty. The marked discrepancy among the three schemes (especially between Morrison and the others) in this study underscored the possible uncertainty associated with R_W. The reliability of the WRF model is heavily dependent on the model-driving initial data provided by mesoscale or global models and complicated scheme setting and parameter adjustment (Liu et al., 2013; Thompson and Eidhammer, 2014; Kumar et al., 2017). However, numerous uncertainties are observed in the parameterization of the WRF simulation, and the choice of microphysical schemes has a significant influence on the inverted DSD (Ćurić et al., 2009; Yang et al., 2019). Therefore, combining the DSDs obtained by an increasing number of disdrometers and the WRF model is valuable. For example, the

Disdrometer Verification Network (DiVeN) in the UK (Pickering et al., 2019) started in Feb 2017 can be introduced to support and improve our estimation in future studies. Moreover, the measurement error by disdrometer may also contaminate the evaluation process. For example, when comparing the observed raindrop velocities based on the disdrometer at Bristol station with their empirical values, we observed dispersion of raindrops, with a number of drops showing significant deviations. This velocity distribution resulted in uncertainty in *ke* estimation.

Soil erosion in the UK is dominated by water erosion (10–30 t km^{-2} yr^{-1}), especially in areas with abundant rainfall in Scotland, where the soil loss rate is approximately 5–10 times that of dry areas (Duck, 1996). Thus, it is significant to estimate rainfall erosivity to elucidate the microphysical characteristics of rainfall and rainfall–soil interactions. Benaud et al. (2020) collated empirical soil erosion observations from UK-based studies into a geodatabase. However, there is a limitation that this database does not cover the entirety of the UK, especially the limited records in northern Scotland. In our future work, we propose to compare the soil loss database with our estimated soil loss using WRF DSD based rainfall erosivity and a soil erosion model (such as RUSLE). We believe that not only can we better analyze the impact of rainfall and rainfall erosivity on the UK soil loss, but also help to better understand microphysical rainfall–soil interactions to support the rational formulation of soil and water conservation planning.

6 Conclusions

This study presented a novel method for large-scale rainfall KE and erosivity estimation based on high-resolution, WRF-derived DSDs. Three microphysical parameterizations schemes (Morrison, WDM6, and Thompson aerosol-aware [TAA]) were designed to obtain raindrop size distributions, rainfall KE and rainfall erosivity for the entire of the UK covering the period of 2013–2017. With validation from the long-term observations of a disdrometer, the WRF-based rainfall erosivity exhibited an acceptable performance at Chilbolton station. Among the three WRF schemes, TAA exhibited the most superior performance and was recommended for future investigation. The results revealed that high rainfall erosivity occurred in the west coast area of the UK. Compared with the traditional empirical method, the proposed method can explain rainfall erosivity from a microphysical perspective and reflect more spatial variation because of changes in rainfall KE at the whole-country scale. Therefore, the development of a numerical weather

prediction model offers an opportunity to better understand rainfall erosivity directly from its true definition. More importantly, because the WRF model is able to be driven by the global reanalysis data to obtain large-scale rainfall kinetic information, the proposed scheme can be easily applied to other regions, especially in ungauged areas.

~~Although an acceptable rainfall erosivity estimation is obtained using the WRF model, some uncertainties associated with it cannot be ignored. For example, as the MPs of WRF were closely related to DSD, improper determination of MPs will introduce additional uncertainty. The marked discrepancy among the three schemes (especially between Morrison and the others) in this study underscored the possible uncertainty associated with R_W. The reliability of the WRF model is heavily dependent on the model-driving initial data provided by mesoscale or global models and complicated scheme setting and parameter adjustment (Liu et al., 2013; Thompson and Eidhammer, 2014; Kumar et al., 2017). However, numerous uncertainties are observed in the parameterization of the WRF simulation, and the choice of microphysical schemes has a significant influence on the inverted DSD (Ćurić et al., 2009; Yang et al., 2019). Therefore, combining the DSDs obtained by an increasing number of disdrometers and the WRF model is valuable. For example, the Disdrometer Verification Network (DiVeN) in the UK (Pickering et al., 2019) started in Feb 2017 can be introduced to support and improve our estimation in future studies. Moreover, the measurement error by disdrometer may also contaminate the evaluation process. For example, when comparing the observed raindrop velocities based on the disdrometer at Bristol station with their empirical values, we observed dispersion of raindrops, with a number of drops showing significant deviations. This velocity distribution resulted in uncertainty in *ke* estimation.~~

~~Soil erosion in the UK is dominated by water erosion (10–30 t km^{-2} yr^{-1}), especially in areas with abundant rainfall in Scotland, where the soil loss rate is approximately 5–10 times that of dry areas (Duck, 1996). Thus, it is significant to estimate rainfall erosivity to elucidate the microphysical characteristics of rainfall and rainfall–soil interactions. Benaud et al. (2020) collated empirical soil erosion observations from UK-based studies into a geodatabase. However, there is a limitation that this database does not cover the entirety of the UK, especially the limited records in northern Scotland. In our future work, we propose to compare the soil loss database with our estimated soil loss using WRF DSD based rainfall erosivity and a soil erosion model (such as RUSLE). We believe that not only can we better analyze the impact of rainfall and rainfall erosivity~~

~~on the UK soil loss, but also help to better understand microphysical rainfall–soil interactions to support the rational formulation of soil and water conservation planning.~~

Some problems remain with the proposed scheme, as discussed in section 5. Some of the problems~~In addition, other sources of uncertainty~~, such as temporal downscaling of rainfall and point-to-area representative error by WRF, may introduce further uncertainty. This should be put in perspective of future work. It is expected that further exploration of research areas with different climatic and geographical characteristics would help us to establish a greater degree of accuracy on this matter.

Author contributions

QD and JZ carried out the experiments, analyzed the data, and prepared the manuscript with contributions from all the co-authors. SLZ modified the text and provided financial support. SNZ carried out quality checks of WRF. GL and DH principally conceived the idea and design of the study.

Competing interests

The authors declare that they have no conflict of interest.

Acknowledgments

This work was supported by the National Natural Science Foundation of China (Nos. 41871299 and 41771424), and the National Key R & D Program of China (Nos. 2018YFB0505500, 2018YFB0505502). The authors acknowledge the British Atmospheric Data Centre and the European Centre for Medium-range Weather Forecasts as the sources of data used in the study.

The rain gauge datasets and Chilbolton disdrometers were sourced from the Met Office Integrated Data Archive System (MIDAS). Both datasets are available from the NCAS British Atmospheric Data Centre (http://archive.ceda.ac.uk/). The ERA-Interim data driving the WRF model can be downloaded from the ECMWF Public Datasets web interface (https://www.ecmwf.int/).

References

Alewell, C., Egli, M. and Meusburger, K. (2015). An attempt to estimate tolerable soil erosion rates by matching soil formation with denudation in Alpine grasslands. Journal of Soils and Sediments 15(6): 1383-1399.

Angulo-Mart ínez, M. and Barros, A. (2015). Measurement uncertainty in rainfall kinetic energy and intensity relationships for soil erosion studies: An evaluation using PARSIVEL disdrometers in the Southern Appalachian Mountains. Geomorphology 228: 28-40.

Angulo-Mart ínez, M., Beguer á, S. and Kysel ý, J. (2016). Use of disdrometer data to evaluate the relationship of rainfall kinetic energy and intensity (KE-I). Science of the Total Environment 568: 83-94.

Angulo-Martinez, M., Beguer á, S., Navas, A. and Machin, J. (2012). Splash erosion under natural rainfall on three soil types in NE Spain. Geomorphology 175: 38-44.

Atlas, D., Srivastava, R. and Sekhon, R. S. (1973). Doppler radar characteristics of precipitation at vertical incidence. Reviews of Geophysics 11(1): 1-35.

Atlas, D. and Ulbrich, C. W. (1977). Path-and area-integrated rainfall measurement by microwave attenuation in the 1–3 cm band. Journal of Applied Meteorology 16(12): 1322-1331.

Ballabio, C., Borrelli, P., Spinoni, J., Meusburger, K., Michaelides, S., Beguer á, S., Klik, A., Petan, S., Janeček, M. and Olsen, P. (2017). Mapping monthly rainfall erosivity in Europe. Science of the Total Environment 579: 1298-1315.

Beard, K. V. (1976). Terminal velocity and shape of cloud and precipitation drops aloft. Journal of the Atmospheric Sciences 33(5): 851-864.

Benaud, P., Anderson, K., Evans, M., Farrow, L., Glendell, M., James, M. R., ... & Brazier, R. E. (2020). National-scale geodata describe widespread accelerated soil erosion. Geoderma, 371: 114378.

Bilotta, G., Grove, M. and Mudd, S. (2012). Assessing the significance of soil erosion. Transactions of the Institute of British Geographers 37(3): 342-345.

Bonta, J. (2004). Development and utility of Huff curves for disaggregating precipitation amounts. Applied Engineering in Agriculture 20(5): 641.

559 Borrelli, P., Robinson, D. A., Fleischer, L. R., Lugato, E., Ballabio, C., Alewell, C., Meusburger,
560 K., Modugno, S., Schütt, B. and Ferro, V. (2017). An assessment of the global impact of 21st
561 century land use change on soil erosion. Nature Communications 8(1): 1-13.

562 Brown, B. R., Bell, M. M. and Frambach, A. J. (2016). Validation of simulated hurricane drop size
563 distributions using polarimetric radar. Geophysical Research Letters 43(2): 910-917.

564 Brown, L. and Foster, G. (1987). Storm erosivity using idealized intensity distributions.
565 Transactions of the ASAE 30(2): 379-386.

566 Carter, C. E., Greer, J., Braud, H. and Floyd, J. (1974). Raindrop characteristics in south central
567 United States. Transactions of the ASAE 17(6): 1033-1037.

568 Cintineo, R., Otkin, J. A., Xue, M. and Kong, F. (2014). Evaluating the performance of planetary
569 boundary layer and cloud microphysical parameterization schemes in convection-permitting
570 ensemble forecasts using synthetic GOES-13 satellite observations. Monthly Weather Review
571 142(1): 163-182.

572 Ćurić, M., Janc, D., Vučković, V. and Kovačević, N. (2009). The impact of the choice of the entire
573 drop size distribution function on Cumulonimbus characteristics. Meteorologische Zeitschrift
574 18(2): 207-222.

575 Dai, Q. and Han, D. (2014). Exploration of discrepancy between radar and gauge rainfall estimates
576 driven by wind fields. Water Resources Research 50(11): 8571-8588.

577 Dai, Q., Bray, M., Zhuo, L., Islam, T., and Han, D. (2017). A scheme for raingauge network design
578 based on remotely-sensed rainfall measurements. Journal of Hydrometeorology 18: 363-379.

579 Dai, Q., Yang, Q., Han, D., Rico‐Ramirez, M. A., and Zhang, S. (2019). Adjustment of radar‐
580 gauge rainfall discrepancy due to raindrop drift and evaporation using the Weather Research and
581 Forecasting model and dual-polarization radar. Water Resources Research 55: 9211–9233.

582 Davison, P., Hutchins, M., Anthony, S., Betson, M., Johnson, C. and Lord, E. (2005). The
583 relationship between potentially erosive storm energy and daily rainfall quantity in England and
584 Wales. Science of the Total Environment 344(1-3): 15-25.

De Roo, A., Wesseling, C. and Ritsema, C. (1996). LISEM: a single‐event physically based hydrological and soil erosion model for drainage basins. I: theory, input and output. Hydrological Processes 10(8): 1107-1117.

Dee, D. P., Uppala, S., Simmons, A., Berrisford, P., Poli, P., Kobayashi, S., Andrae, U., Balmaseda, M., Balsamo, G. and Bauer, d. P. (2011). The ERA‐Interim reanalysis: Configuration and performance of the data assimilation system. Quarterly Journal of the Royal Meteorological Society 137(656): 553-597.

Defra (2009). Safeguarding our soils–A strategy for England. Defra, UK.

Doelling, I. G., Joss, J. and Riedl, J. (1998). Systematic variations of Z–R-relationships from drop size distributions measured in northern Germany during seven years. Atmospheric Research 47: 635-649.

Duck, R. W. (1996). Regional variations of fluvial sediment yield in eastern Scotland. Erosion and Sediment Yield: Global and Regional Perspectives 236:157-161.

Dudhia, J. (1989). Numerical study of convection observed during the winter monsoon experiment using a mesoscale two-dimensional model. Journal of the Atmospheric Sciences 46(20): 3077-3107.

EA (2004). The state of soils in England and Wales. Environment Agency, UK.

Ek, M., Mitchell, K., Lin, Y., Rogers, E., Grunmann, P., Koren, V., Gayno, G. and Tarpley, J. (2003). Implementation of Noah land surface model advances in the National Centers for Environmental Prediction operational mesoscale Eta model. Journal of Geophysical Research: Atmospheres 108(22):8851.

Evans, R. (1990). Soils at risk of accelerated erosion in England and Wales. Soil use and Management 6(3): 125-131.

Fornis, R. L., Vermeulen, H. R. and Nieuwenhuis, J. D. (2005). Kinetic energy–rainfall intensity relationship for Central Cebu, Philippines for soil erosion studies. Journal of Hydrology 300(1-4): 20-32.

611 Gilmore, M. S., Straka, J. M. and Rasmussen, E. N. (2004). Precipitation uncertainty due to
612 variations in precipitation particle parameters within a simple microphysics scheme. Monthly
613 Weather Review 132(11): 2610-2627.

614 Hanel, M., Máca, P., Bašta, P., Vlnas, R. and Pech, P. (2016). The rainfall erosivity factor in the
615 Czech Republic and its uncertainty. Hydrology and Earth System Sciences 20(10): 4307-4322.

616 Hong, S.-Y., Lim, K.-S. S., Lee, Y.-H., Ha, J.-C., Kim, H.-W., Ham, S.-J. and Dudhia, J. (2010).
617 Evaluation of the WRF double-moment 6-class microphysics scheme for precipitating convection.
618 Advances in Meteorology 2010.

619 Hudson, N. (1963). Raindrop size distribution in high intensity storms. Rhodesian Journal of
620 Agricultural Research 1(1): 6-11.

621 Islam, T., Rico-Ramirez, M. A., Thurai, M. and Han, D. (2012). Characteristics of raindrop spectra
622 as normalized gamma distribution from a Joss–Waldvogel disdrometer. Atmospheric Research
623 108: 57-73.

624 Janjić, Z. I. (1994). The step-mountain eta coordinate model: Further developments of the
625 convection, viscous sublayer, and turbulence closure schemes. Monthly Weather Review 122(5):
626 927-945.

627 Johnson, M., Jung, Y., Dawson, D. T. and Xue, M. (2016). Comparison of simulated polarimetric
628 signatures in idealized supercell storms using two-moment bulk microphysics schemes in WRF.
629 Monthly Weather Review 144(3): 971-996.

630 Jones, D. M. A. (1959). The shape of raindrops. Journal of the Atmospheric Sciences 16(1): 511-
631 515.

632 Jung, Y., Xue, M. and Zhang, G. (2010). Simulations of polarimetric radar signatures of a supercell
633 storm using a two-moment bulk microphysics scheme. Journal of Applied Meteorology and
634 Climatology 49(1): 146-163.

635 Kain, J. S. (2004). The Kain–Fritsch convective parameterization: an update. Journal of Applied
636 Meteorology 43(1): 170-181.

637 Kinnell, P. (1981). Rainfall intensity-kinetic energy relationships for soil loss prediction. Soil
638 Science Society of America Journal 45(1): 153-155.

Kinnell, P. and Risse, L. (1998). USLE-M: empirical modeling rainfall erosion through runoff and sediment concentration. Soil Science Society of America Journal 62(6): 1667-1672.

Lim, K.-S. S. and Hong, S.-Y. (2010). Development of an effective double-moment cloud microphysics scheme with prognostic cloud condensation nuclei (CCN) for weather and climate models. Monthly Weather Review 138(5): 1587-1612.

Lim, Y. S., Kim, J. K., Kim, J. W., Park, B. I. and Kim, M. S. (2015). Analysis of the relationship between the kinetic energy and intensity of rainfall in Daejeon, Korea. Quaternary International 384: 107-117.

Marshall, J. S. and Palmer, W. M. K. (1948). The distribution of raindrops with size. Journal of Meteorology 5(4): 165-166.

McIsaac, G. (1990). Apparent geographic and atmospheric influences on raindrop sizes and rainfall kinetic energy. Journal of Soil and Water Conservation 45(6): 663-666.

Meshesha, D. T., Tsunekawa, A. and Haregeweyn, N. (2019). Influence of raindrop size on rainfall intensity, kinetic energy, and erosivity in a sub-humid tropical area: a case study in the northern highlands of Ethiopia. Theoretical and Applied Climatology 136(3-4): 1221-1231.

Meshesha, D. T., Tsunekawa, A., Tsubo, M., Haregeweyn, N. and Adgo, E. (2014). Drop size distribution and kinetic energy load of rainfall events in the highlands of the Central Rift Valley, Ethiopia. Hydrological Sciences Journal 59(12): 2203-2215.

Meshesha, D. T., Tsunekawa, A., Tsubo, M., Haregeweyn, N. and Tegegne, F. (2016). Evaluation of kinetic energy and erosivity potential of simulated rainfall using Laser Precipitation Monitor. Catena 137: 237-243.

Mikoš, M., Jošt, D. and Petkovšek, G. (2006). Rainfall and runoff erosivity in the alpine climate of north Slovenia: a comparison of different estimation methods. Hydrological sciences journal 51(1): 115-126.

Mlawer, E. J., Taubman, S. J., Brown, P. D., Iacono, M. J. and Clough, S. A. (1997). Radiative transfer for inhomogeneous atmospheres: RRTM, a validated correlated ‐ k model for the longwave. Journal of Geophysical Research: Atmospheres 102(14): 16663-16682.

MO (2012). Met Office Integrated Data Archive System (MIDAS) land and marine surface stations data (1853 - current).

Montopoli, M., Marzano, F. S. and Vulpiani, G. (2008). Analysis and synthesis of raindrop size distribution time series from disdrometer data. IEEE Transactions on Geoscience and Remote Sensing 46(2): 466-478.

Morgan, R. (1985). Assessment of soil erosion risk in England and Wales. Soil use and Management 1(4): 127-131.

Morrison, H., Milbrandt, J. A., Bryan, G. H., Ikeda, K., Tessendorf, S. A. and Thompson, G. (2015). Parameterization of cloud microphysics based on the prediction of bulk ice particle properties. Part II: Case study comparisons with observations and other schemes. Journal of the Atmospheric Sciences 72(1): 312-339.

Morrison, H., Thompson, G. and Tatarskii, V. (2009). Impact of cloud microphysics on the development of trailing stratiform precipitation in a simulated squall line: Comparison of one-and two-moment schemes. Monthly weather review 137(3): 991-1007.

Naipal, V., Reick, C. H., Pongratz, J. and Van Oost, K. (2015). Improving the global applicability of the RUSLE model-adjustment of the topographical and rainfall erosivity factors. Geoscientific Model Development 8: 2893-2913.

Nyssen, J., Vandenreyken, H., Poesen, J., Moeyersons, J., Deckers, J., Haile, M., Salles, C. and Govers, G. (2005). Rainfall erosivity and variability in the Northern Ethiopian Highlands. Journal of Hydrology 311(1-4): 172-187.

O'Neill, D. (2007). The total external environmental costs and benefits of agriculture in the UK. Environment Agency, UK.

Panagos, P., Ballabio, C., Borrelli, P., Meusburger, K., Klik, A., Rousseva, S., Tadić, M. P., Michaelides, S., Hrabal ĭkov á, M. and Olsen, P. (2015a). Rainfall erosivity in Europe. Science of the Total Environment 511: 801-814.

Panagos, P., Borrelli, P., Meusburger, K., Yu, B., Klik, A., Lim, K. J., Yang, J. E., Ni, J., Miao, C. and Chattopadhyay, N. (2017). Global rainfall erosivity assessment based on high-temporal resolution rainfall records. Scientific reports 7(1): 1-12.

694 Panagos, P., Borrelli, P., Poesen, J., Ballabio, C., Lugato, E., Meusburger, K., Montanarella, L.
695 and Alewell, C. (2015b). The new assessment of soil loss by water erosion in Europe.
696 Environmental Science & Policy 54: 438-447.

697 Park, S., Mitchell, J. and Bubenzer, G. (1982). Splash erosion modeling: physical analysis.
698 Transactions of the ASAE 25:357-361.

699 Petan, S., Rusjan, S., Vidmar, A. and Mikoš, M. (2010). The rainfall kinetic energy–intensity
700 relationship for rainfall erosivity estimation in the mediterranean part of Slovenia. Journal of
701 Hydrology 391(3-4): 314-321.

702 Pickering, B. S., Neely III, R. R., & Harrison, D. (2019). The Disdrometer Verification Network
703 (DiVeN): a UK network of laser precipitation instruments. Atmospheric Measurement Techniques
704 12: 5845-5861.

705 Prigent, C. (2010). Precipitation retrieval from space: An overview. Comptes Rendus Geoscience
706 342(4-5): 380-389.

707 Renard, K. G., Foster, G. R., Weesies, G., McCool, D. and Yoder, D. (1997). Predicting soil
708 erosion by water: a guide to conservation planning with the Revised Universal Soil Loss Equation
709 (RUSLE), United States Department of Agriculture Washington, DC.

710 Rosewell, C. J. (1986). Rainfall kinetic energy in eastern Australia. Journal of Climate and Applied
711 Meteorology 25(11): 1695-1701.

712 Sanchez-Moreno, J. F., Mannaerts, C. M., Jetten, V. and Löffler-Mang, M. (2012). Rainfall kinetic
713 energy–intensity and rainfall momentum–intensity relationships for Cape Verde. Journal of
714 Hydrology 454: 131-140.

715 Sempere‐Torres, D., Porrà, J. M. and Creutin, J. D. (1998). Experimental evidence of a general
716 description for raindrop size distribution properties. Journal of Geophysical Research:
717 Atmospheres 103(2): 1785-1797.

718 Song, Y., Han, D. and Rico-Ramirez, M. A. (2017). High temporal resolution rainfall rate
719 estimation from rain gauge measurements. Journal of Hydroinformatics 19(6): 930-941.

720 Thompson, G. and Eidhammer, T. (2014). A study of aerosol impacts on clouds and precipitation
721 development in a large winter cyclone. Journal of the Atmospheric Sciences 71(10): 3636-3658.

Uplinger, W. (1981). A new formula for raindrop terminal velocity. Conference on Radar Meteorology, 20 th, Boston, MA.

Van Dijk, A., Bruijnzeel, L. and Rosewell, C. (2002). Rainfall intensity–kinetic energy relationships: a critical literature appraisal. Journal of Hydrology 261(1-4): 1-23.

Wang, L., Shi, Z., Wang, J., Fang, N., Wu, G. and Zhang, H. (2014). Rainfall kinetic energy controlling erosion processes and sediment sorting on steep hillslopes: a case study of clay loam soil from the Loess Plateau, China. Journal of Hydrology 512: 168-176.

Weiss, L. L. (1964). Ratio of true to fixed-interval maximum rainfall. Journal of the Hydraulics Division 90(1): 77-82.

Williams, R. and Sheridan, J. (1991). Effect of rainfall measurement time and depth resolution on EI calculation. Transactions of the ASAE 34(2): 402-0406.

Wischmeier, W. H. and Smith, D. D. (1958). Rainfall energy and its relationship to soil loss. Eos, Transactions American Geophysical Union 39(2): 285-291.

Wischmeier, W. H. and Smith, D. D. (1978). Predicting rainfall erosion losses-a guide to conservation planning. Department of Agriculture, Science and Education Administration, US.

Xie, Y., Yin, S., Liu, B., Nearing, M. A. and Zhao, Y. (2016). Models for estimating daily rainfall erosivity in China. Journal of Hydrology 535: 547-558.

Yang, Q., Dai, Q., Han, D., Chen, Y., and Zhang, S. (2019). Sensitivity analysis of raindrop size distribution parameterizations in weather research and forecasting rainfall simulation. Atmospheric Research 228:1-13.

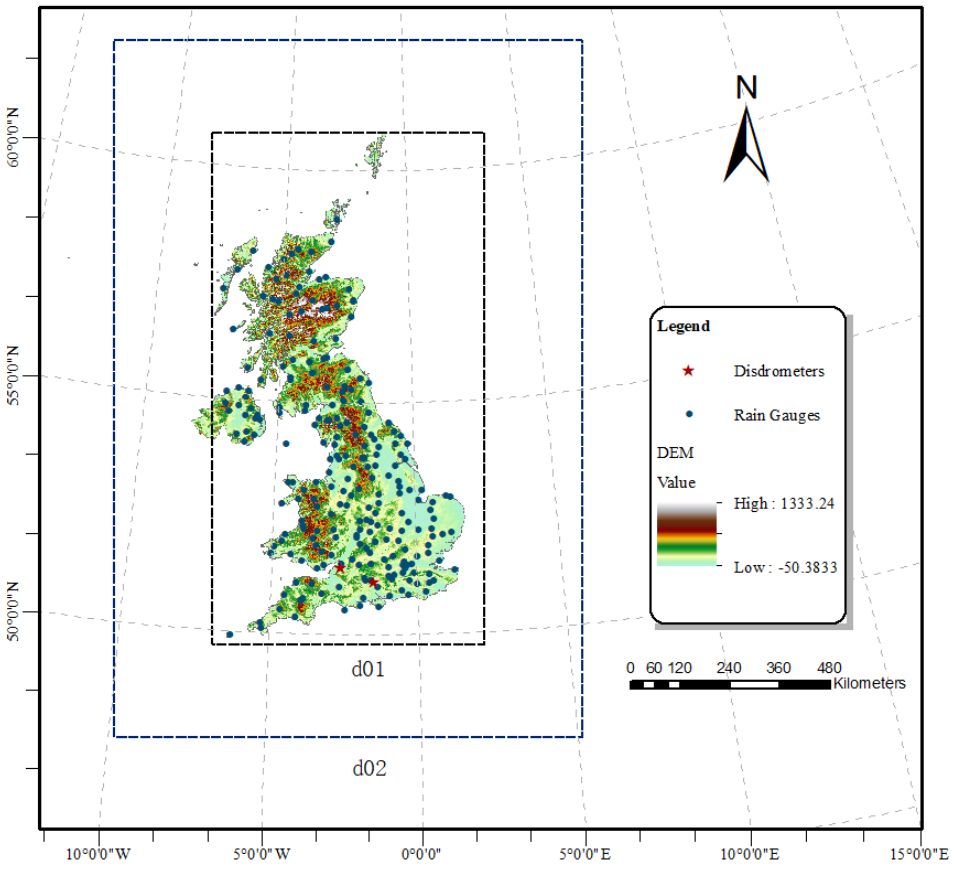

744

745 **Figure 1**. Location of rain gauges, Joss–Waldvogel disdrometer (JWD) at Chilbolton Observatory,
746 OTT Parsivel^2 disdrometer (OPD) at Bristol Observatory and configurations of domain setups in
747 the WRF model.

748

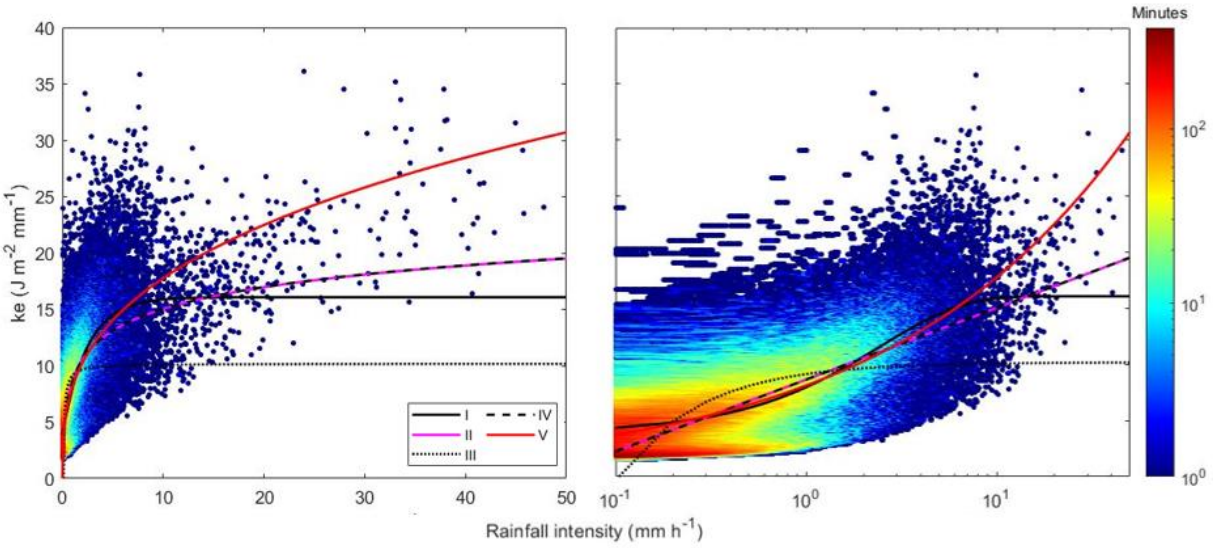

749

750 **Figure 2**. Minutes number per intensity class (x-axis) and *ke* class (y-axis) with five fitted *ke–I*
751 curves at Chilbolton station (2004–2013), plotted on linear (left) and logarithmic (right) intensity
752 scales.

753

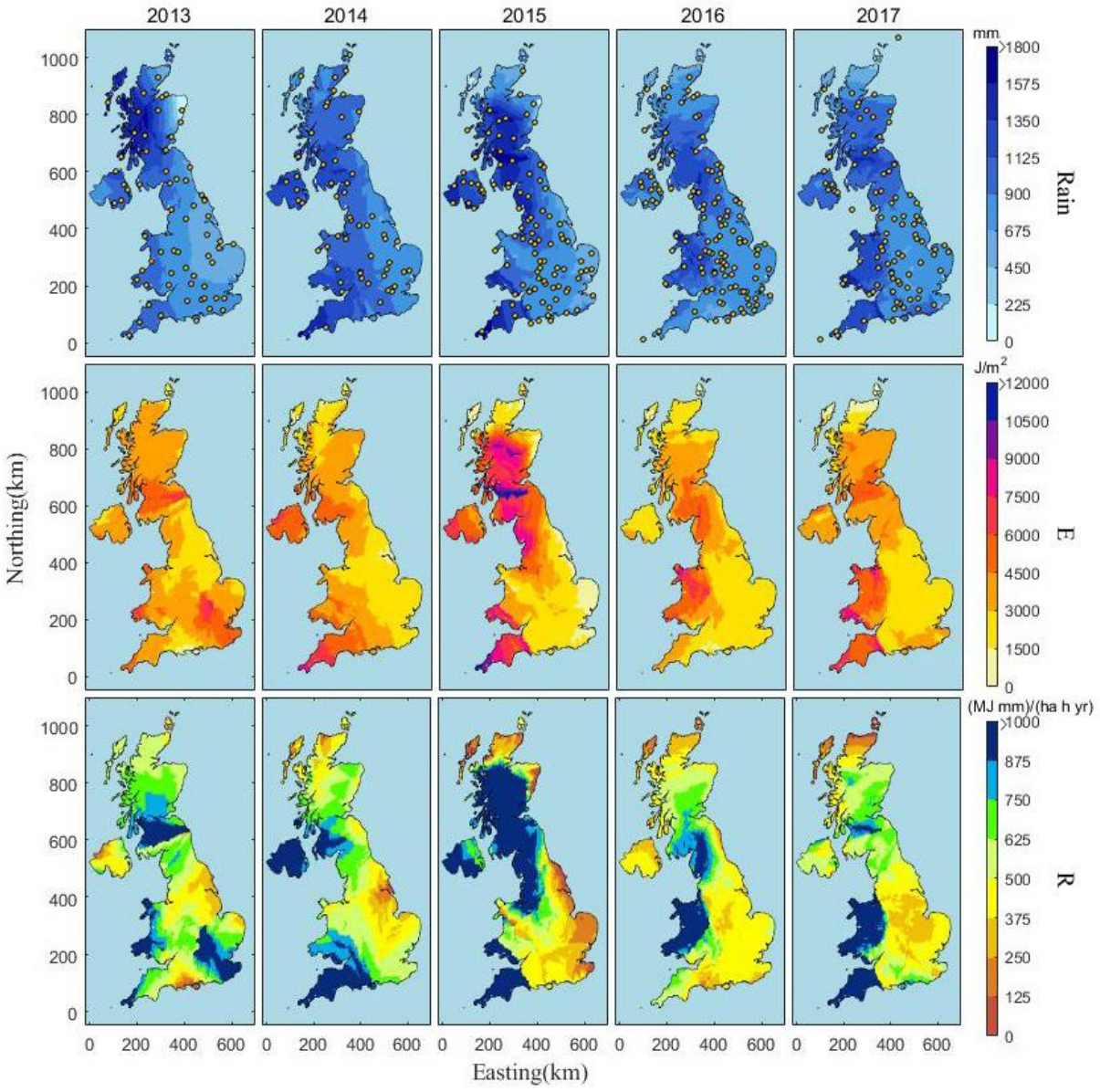

754

755 **Figure 3**. Gauge-based interpolation maps of annual rainfall amount (*Rain*), rainfall kinetic energy
756 (*E*) and rainfall erosivity (*R*) in 2013–2017.

757

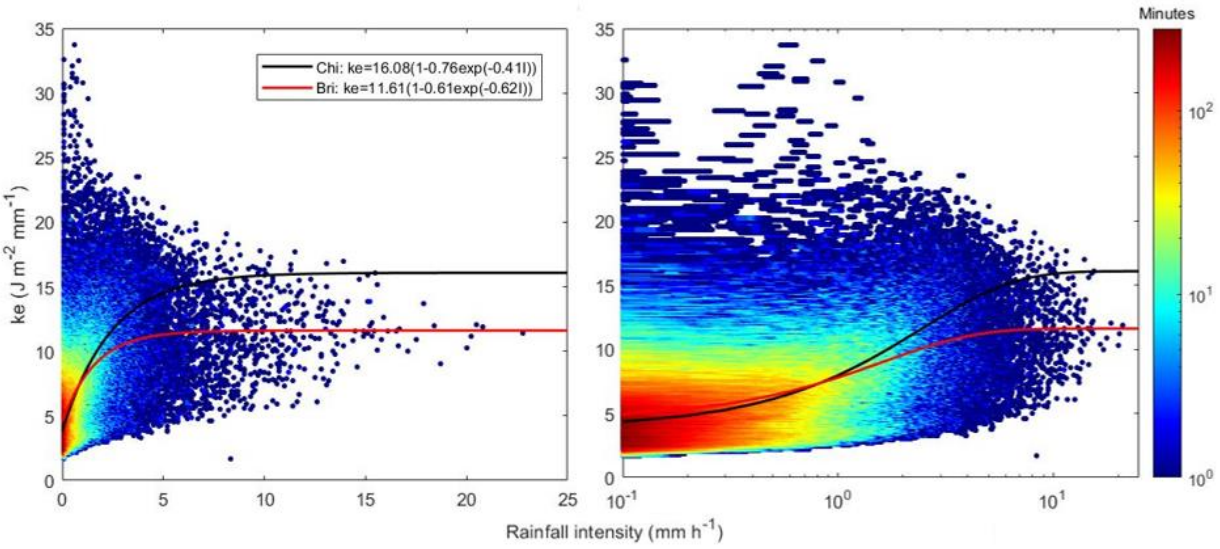

758

759 **Figure 4**. Minutes number per intensity class (x-axis) and ke class (y-axis) with fitted *ke–I* curves
760 at Bristol station (2015–2018), plotted on linear (left) and logarithmic (right) intensity scales.

761

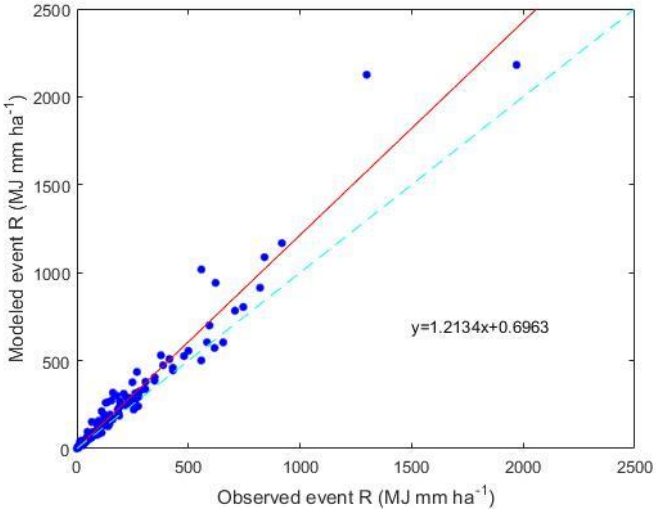

762

763 **Figure 5**. Comparison of observed and modeled event rainfall erosivity at Bristol Station, covering
764 the period of 2016–2019.

765

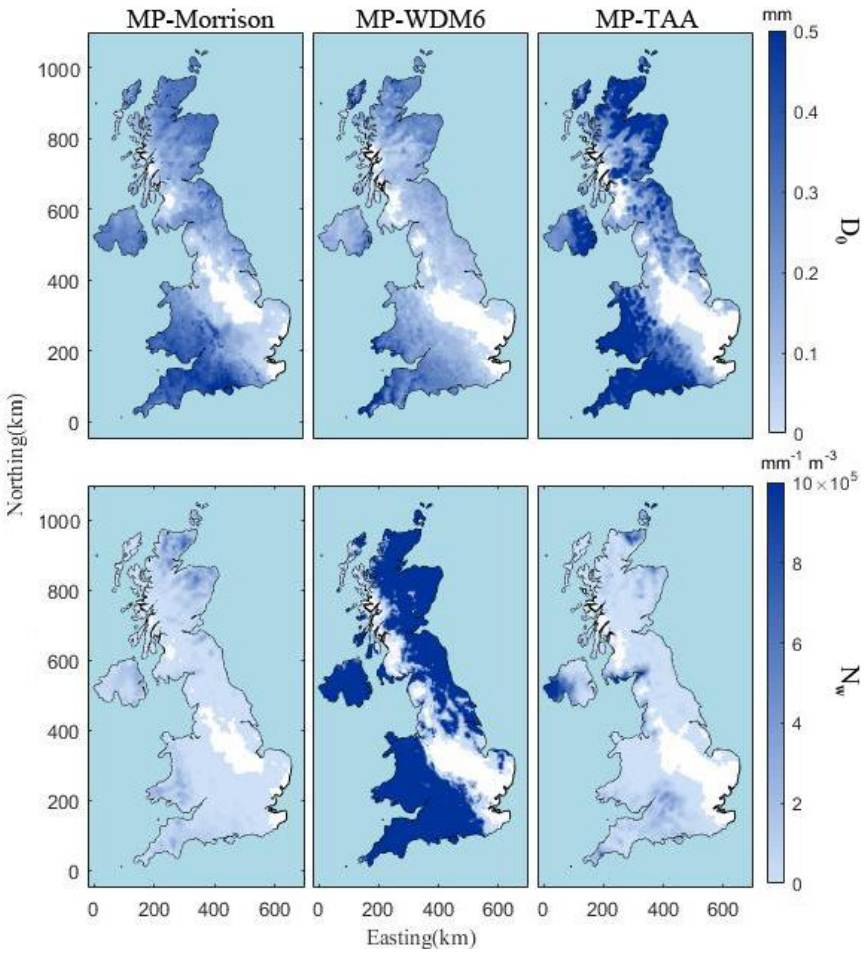

766

767 **Figure 6**. Map of average WRF DSD D_0 and N_w (January 10, 2013).

768

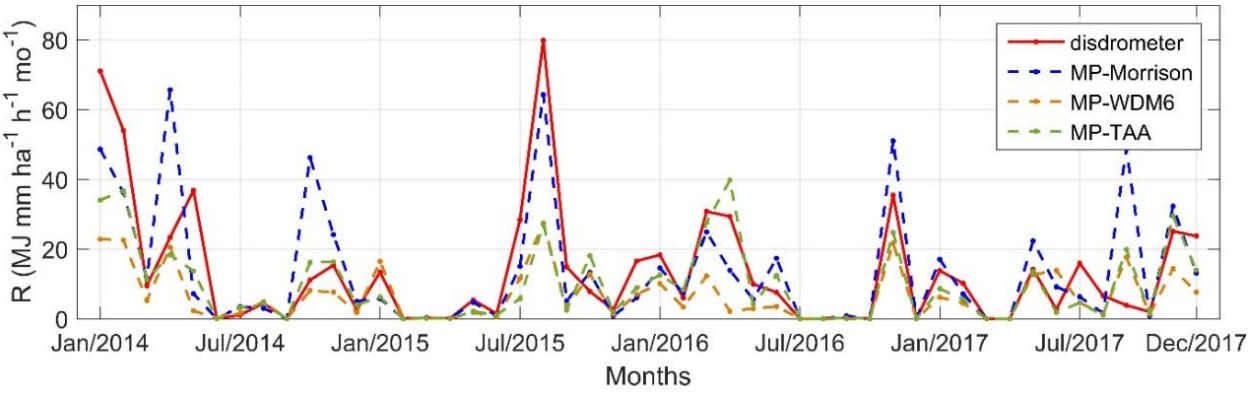

769

770 **Figure 7**. Comparison of disdrometer- and WRF-derived monthly rainfall erosivity estimations at
771 Chilbolton station (2014–2017).

772

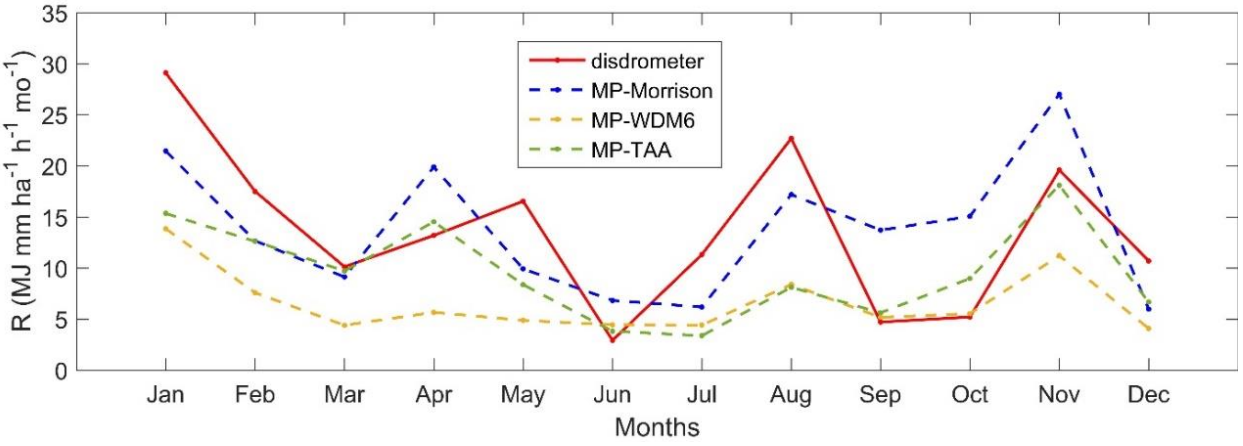

773

774 **Figure 8**. Comparison of disdrometer- and WRF-derived average monthly rainfall erosivity
775 estimations at Chilbolton station (2014–2017).

776

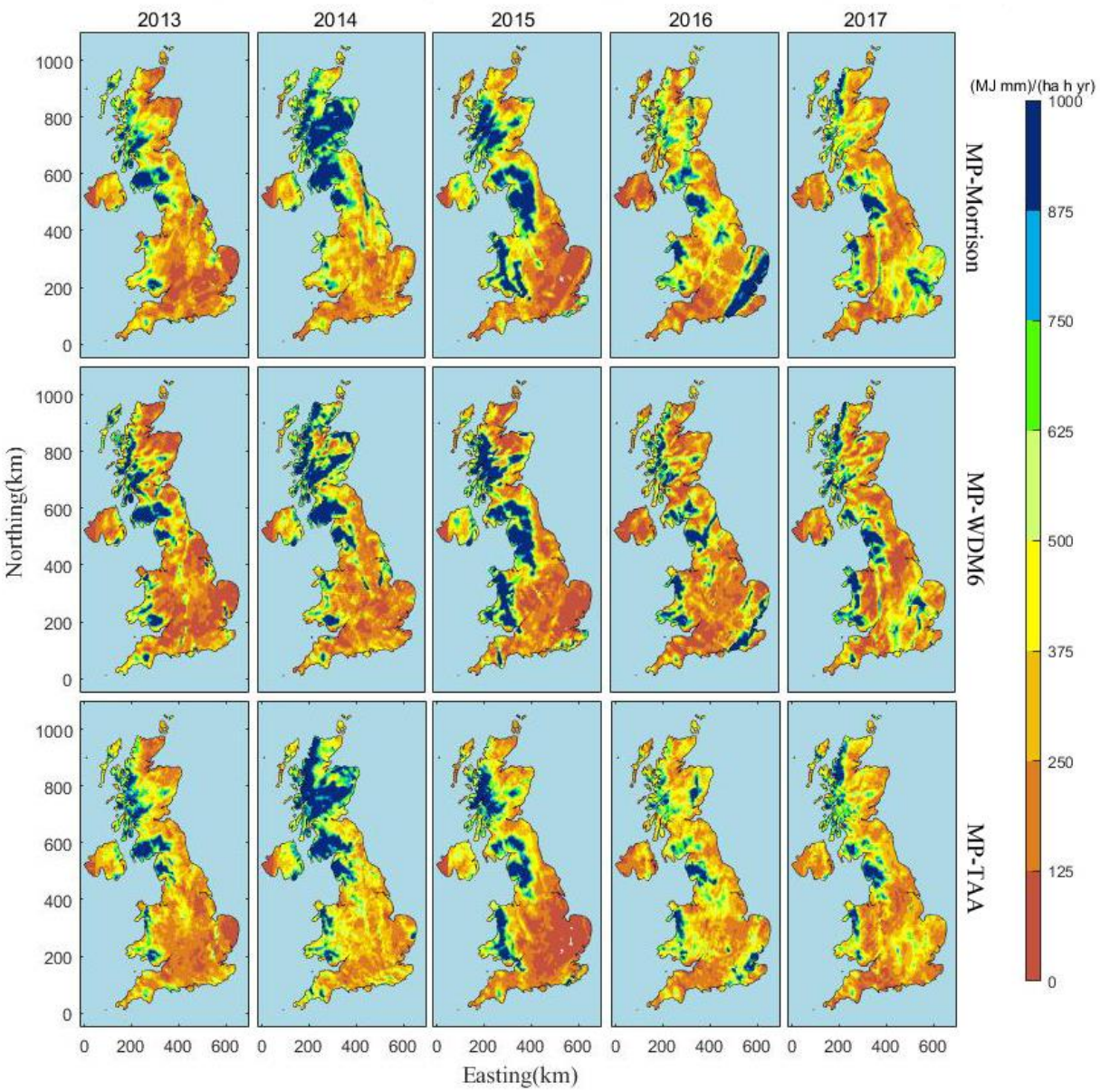

777
778 **Figure 9**. WRF-derived annual rainfall erosivity maps of the whole UK for different years.

779

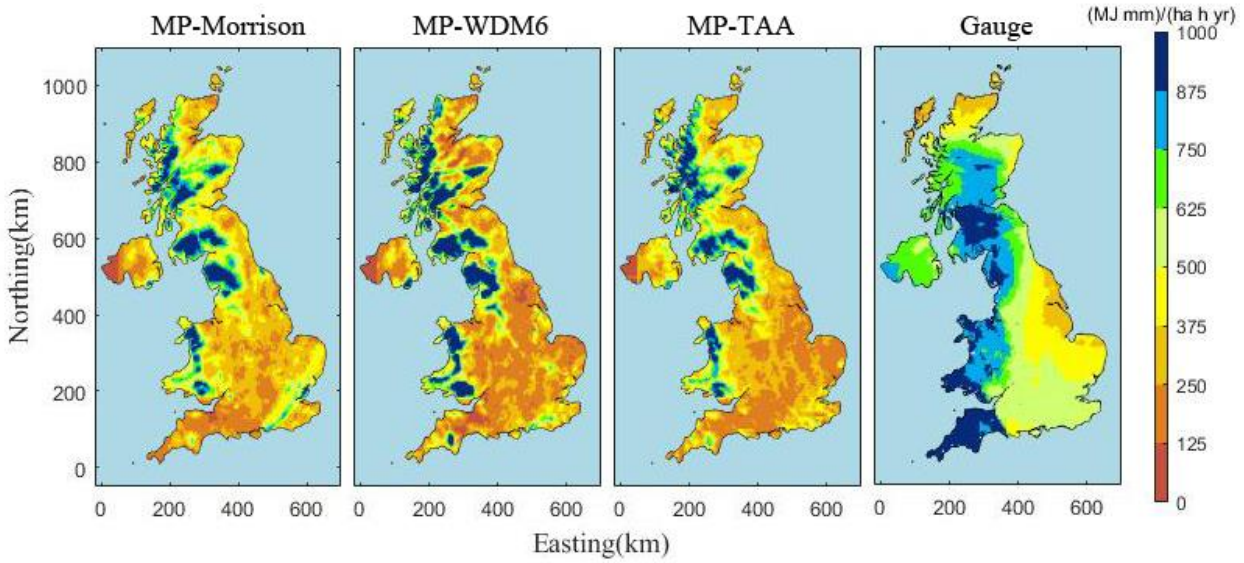

780

781 **Figure 10**. The 5-year (2013–2017) average annual rainfall erosivity maps based on WRF grids
782 and rain gauge interpolation.

783

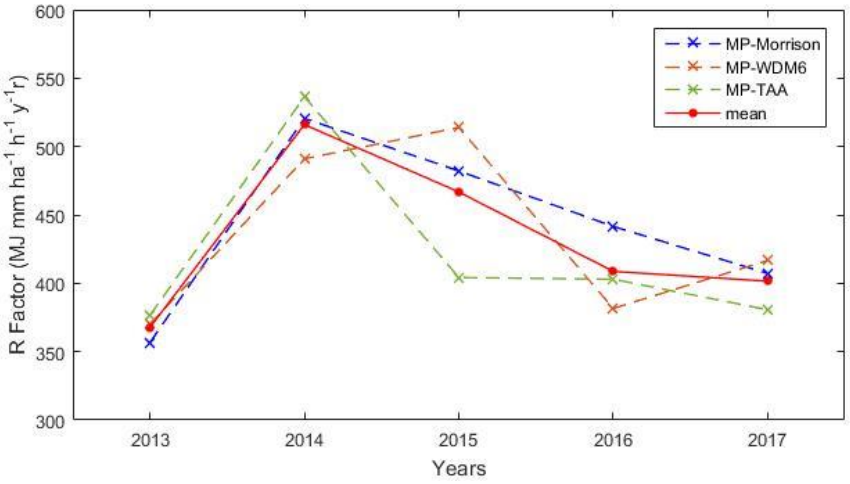

784

785 **Figure 11**. WRF-derived average annual rainfall erosivity of all the WRF grids covering the whole
786 UK (2013–2017).

787

788 **Table 1.** Relationship of *ke–I* at Chilbolton Station (2004–2013).

ID	Equation	Calibration R^2	Validation R^2
I	$ke = 16.08(1 - 0.76e^{-0.41I})$	0.50	0.45
II	$ke = 8.65 + 6.39\lg(I)$	0.48	0.43
III	$ke = 10.19 - 1.05/I$	0.29	0.25
IV	$ke = 8.65 + 2.78\ln(I)$	0.48	0.43
V	$ke = 8.12I^{0.34}$	0.50	0.45

789

790

Table 2. The configurations of WRF model for two nested domains.

Domain	Domain size (km)	Grid Spacing (km)	Grid size	Downscaling ratio
d01	1,125 × 1,675	25	45 × 67	-
d02	655 × 1,230	5	131 × 246	1:5

Table 3. Indicators comparison between disdrometer-derived rainfall erosivity R_D and three types of WRF-derived rainfall erosivity at Chilbolton station on monthly scale (2014-2017).

Indicators	MP-Morrison	MP-WDM6	MP-TAA
Pearson	0.71	0.77	0.79
MAE	8.05	8.42	6.51
R^2	0.42	0.31	0.54